Biogeosciences Discuss., 12, 5725–5756, 2015
www.biogeosciences-discuss.net/12/5725/2015/
doi:10.5194/bgd-12-5725-2015
© Author(s) 2015. CC Attribution 3.0 License.

Biogeosciences Discussions
Open Access

This discussion paper is/has been under review for the journal Biogeosciences (BG).
Please refer to the corresponding final paper in BG if available.

Seasonal characterization of CDOM for lakes in semi-arid regions of Northeast China using excitation-emission matrices fluorescence and parallel factor analysis (EEM-PARAFAC)

Y. Zhao[1], K. Song[1], Z. Wen[1], L. Li[2], S. Zang[3], T. Shao[1], S. Li[1], and J. Du[1]

[1]Northeast Institute of Geography and Agroecology, Chinese Academy of Sciences, Changchun, Jilin, 130102, China
[2]Department of Earth Sciences, Indiana University-Purdue University, Indianapolis, IN, USA
[3]College of Geographical Science, Harbin Normal University, Harbin, China

Received: 28 October 2014 – Accepted: 15 November 2014 – Published: 15 April 2015

Correspondence to: K. Song (songks@iga.ac.cn)

Published by Copernicus Publications on behalf of the European Geosciences Union.

Abstract

The seasonal characteristics of fluorescence components in CDOM for lakes in the semi-arid region of Northeast China were examined by excitation-emission matrices fluorescence and parallel factor analysis (EEM-PARAFAC). Two humic-like peaks C1 (Ex/Em = 230, 300/425 nm) and C2 (Ex/Em = 255, 350/460 nm) and two protein-like B (Ex/Em = 220, 275/320 nm) and T (Ex/Em = 225, 290/360 nm) peaks were identified using PARAFAC. The average fluorescence intensity of the four components differed with seasonal variation from June and August 2013 to February and April 2014. The total fluorescence intensity significantly varied from $2.54 \pm 0.68\,nm^{-1}$ in June to the mean value $1.93 \pm 0.70\,nm^{-1}$ in August 2013, and then increased to $2.34 \pm 0.92\,nm^{-1}$ in February and reduced to the lowest $1.57 \pm 0.55\,nm^{-1}$ in April 2014. In general, the fluorescence intensity was dominated by peak C1, indicating that most part of CDOM for inland waters being investigated in this study was originated from phytoplankton degradation. The lowest C2 represents only a small portion of CDOM from terrestrial imported organic matter to water bodies through rainwash and soil leaching. The two protein-like intensities (B and T) formed in situ through microbial activity have almost the same intensity. Especially, in August 2013 and February 2014, the two protein-like peaks showed obviously difference from other seasons and the highest C1 ($1.02\,nm^{-1}$) was present in February 2014. Components 1 and 2 exhibited strong linear correlation ($R^2 = 0.633$). There were significantly positive linear relationships between CDOM absorption coefficients a(254) ($R^2 = 0.72$, 0.46, $p < 0.01$), a(280) ($R^2 = 0.77$, 0.47, $p < 0.01$), a(350) ($R^2 = 0.76$, 0.78, $p < 0.01$) and F_{max} for two humic-like components (C1 and C2), respectively. A close relationship ($R^2 = 0.931$) was found between salinity and DOC. However, almost no obvious correlation was found between salinity and EEM-PARAFAC extracted components except for C3 ($R^2 = 0.469$). Results from this investigation demonstrate that the EEM-PARAFAC technique can be used to evaluate the seasonal dynamics of CDOM fluorescence components for inland waters in semi-arid regions of Northeast China.

BGD
12, 5725–5756, 2015

1 Introduction

Dissolved organic matter (DOM), a heterogeneous mixture of humic acid, proteinaceous and carbohydrates, plays an array of important roles in aquatic ecosystems (Zhang et al., 2010). Chromophoric dissolved organic matter (CDOM), the colored fraction of DOM, absorbs light energy in the UV (280–400 nm) and blue region of the spectrum and inhibits the propagation of ultraviolet radiation. CDOM in waters also affects the transport and bio-availability of materials such as trace metals and other pollutants (Song et al., 2013), so it can be used as a proxy of water quality. In natural water bodies, CDOM originates from the degradation of plant materials and terrestrial imported substance, which varies in time and space and is controlled by the structure and composition (Stedmon et al., 2003). CDOM is compositionally complex, which makes it difficult to isolate hydrophobic and hydrophilic acid using XAD ion-exchange resins (Aiken et al., 1992; Spencer et al., 2010). Nonetheless, some optically active components (OACs) of CDOM can be excited by certain wavelengths and re-emit fluorescence (Zhang et al., 2010) so that the fluorescence spectroscopic techniques such as fluorescence emission spectrometry, synchronous fluorescence scanning (SFS) and excitation-emission matrix fluorescence spectroscopy (EEMs) can be used to provide detailed information about the source and concentration of CDOM. Generally, surface waters contain two key fluorescence components originated from CDOM: humic-like and protein-like substances (Coble, 1996; Fellman et al., 2010; Guo et al., 2010; Hudson et al., 2007; Stedmon et al., 2003; Zhang et al., 2010).

When a molecule absorbs light energy, a loosely held electron is excited and promoted to a higher energy unoccupied orbit, and then the CDOM fluorescence occurs when the electron returns to the ground state. Some energy is lost from the excited state to ground state by collision (fluorescence quenching) and non-radiative decay including vibrational relaxation and internal conversion, resulting in the emission energy lower than the excitation energy (the Stokes' Shift). The fluorescence signatures are dependent on the structure of chemical molecules that can absorb and re-emit light

BGD
12, 5725–5756, 2015

energy as well as other factors such as temperature or pH of the solution (Hudson et al., 2007; Stedmon et al., 2003).

Traditional fluorescence techniques including fluorescence emission spectrometry and synchronous fluorescence scanning applied to study CDOM components have the drawback that the output was restricted to a linear scan (Hudson et al., 2007). Recently, the fluorescence excitation-emission matrix spectroscopy (EEMs) was applied to identify CDOM components which provide abundant information of synchronous scan spectra in the form of contours (Coble, 1996). The EEMs is considered the simplest and most effective technique for studying the composition of fluorophores given its high selectivity and sensitivity to CDOM in water columns (Zhang et al., 2010). In recent years, fluorescence spectroscopy has been widely used to distinguish allochthonous (humic-like fluorophores) and autochthonous (protein-like fluorophores) CDOM source in coastal environment (Coble et al., 1998; Mayer et al., 1999; Yamashita et al., 2008, 2010; Zhang et al., 2013) and to investigate the dynamics of various aquatic ecosystem including marine, freshwaters and snow, ice-water systems (Barker et al., 2006, 2009, 2010, 2013; Coble, 2007; Hudson et al., 2007; Stedmon et al., 2007). Based on the peak positions in EEM, two main fluorescence components, i.e., humic-like and protein-like (Peaks B and T) substance have been identified and investigated (DelCastillo et al., 1999; Jaffé et al., 2004). However, because of overlapped fluorophores of CDOM EEMs, the traditional "peak-picking" method may be unreliable to evaluate CDOM dynamics in aquatic ecosystems (Coble, 1996; Stedmon et al., 2003). Recently, the combined EEMs-PARAFAC (parallel factor analysis) technique has been shown to effectively decompose EEM of CDOM into independent fluorescent component and assess the source of CDOM and relationships with other water quality parameters (Broisover et al., 2009; Guo et al., 2010; Zhang et al., 2010, 2011, 2013). Stedmon et al. (2003) introduced parallel factor analysis (PARAFAC) to decompose EEMs into individual fluorescent components. Their investigation identified five distinct DOM components for a Danish estuary and its catchment (Stedmon et al., 2003). In coastal environments, Yamashita (2008) reported on seven components using the combined

BGD
12, 5725–5756, 2015

EEMs-PARAFAC technique and assess the dynamic of individual fluorophores and relationship with salinity in Ise Bay. Zhang et al. (2011) also found three different components by PARAFAC model and analyzed the correlations the fluorescence components and the absorption coefficients of CDOM for Lake Tianmu and its catchment.

Compared with fresh waters, Song et al. (2013) found that the brackish waters (salinity $\geq$ 0.55 PSU) exhibited high average DOC concentration contributing significantly to the carbon budget for inland waters, small average $SUVA_{254}$ and high average S_R indicating large portion of lower molecules in DOC in the Songnen Plain. As suggested by Duarte et al. (2008) and Tranvik et al. (2009), a huge amount of DOC may store in these brackish waters. Therefore, it motivated us to investigate the components of fresh and brackish waters furthermore in the semi-arid region. To achieve this goal, 67 water samples were collected from seven lakes in the western part of Jilin province in different seasons and the absorption and fluorescence of CDOM were determined for these water samples. The specific objectives of this study are to: (1) characterize CDOM components contained in both saline and fresh water lakes using EEMs and their origins through the EEM-PARAFAC method, (2) assess the dynamic of individual fluorescence component of CDOM with seasonal variations, and most importantly (3) link CDOM fluorescence intensity and the absorption coefficients, DOC concentration and salinity as well.

2 Materials and methods

2.1 Lakes and water sampling

The water bodies to be investigated in this study were located in the western part of Jilin Province, which belongs to the semi-arid part of the Songnen Plain (Song et al., 2013). Two group of lakes were investigated, i.e., the Chagan lake group and the Yuelianghu lake group. The Chagan lake group is made up of Lake Chagan (CGL), Xinmiaopao

BGD
12, 5725–5756, 2015

(XMP), Xindianpao (XDP) and Kulipao (KLP) with the mean high salinity 0.55 PSU. The Yuelianghu lake group mainly includes Lake Yueliang (YLL), Talahong (TLH) and Xinhuangpao (XHP) with the average salinity 0.33 PSU (Fig. 1). The primary economic value for these lakes is related to fishery, agricultural irrigation and recreation. For the study region, the average annual precipitation is 391 mm, but the average evaporation reaches to 1790 mm, resulting in water scarcity. Due to the area dominated by saline-alkali soil, the rainfall flush and agricultural practice can result in an increase of lake salinities. In order to characterize the CDOM fluorescence components with seasonal variation through EEMs-PARAFAC, 67 water samples were collected from the surface of the seven lakes in 1 L acid-cleaned plastic bottles for four field campaigns in July, August 2013 and February, April 2014, respectively. The collected samples were held on ice and immediately transported to the laboratory in Changchun City of Jilin province within 3 h. In the laboratory, these samples were kept at 4 °C until analysis within two days. Latitude and longitude of each sample location were recorded in situ using a Trimble Global Positioning System (GPS).

2.2 Analytical procedures

To characterize the basic parameters of water quality, salinity was measured through a DDS-307 electrical conductivity (EC) meter with the $\mu S\,cm^{-1}$ (micro-Siemens/centimeter) unit at room temperature (20 ± 2 °C) in laboratory. Salinity was expressed on the basis of the UNESCO practical salinity Unit (PSU 1978). The pH was measured using a PHS-3C pH meter at room temperature (20 ± 2 °C) in laboratory. Water turbidity was determined using a Shimadzu UV-2600PC UV-Vis dual beam spectrophotometer with matching 3 cm quartz cells at room temperature (20 ± 2 °C) with Milli-Q water as the reference.

BGD
12, 5725–5756, 2015

2.3 DOC concentration measurement

To determine DOC concentrations, water samples were filtered through pre-combusted 0.45 µm Whatman GF/F filters and then were measured using a Shimadzu TOC-5000 Analyzer and a 1.2 % Pt on silica catalyst at 680 °C. Potassium hydrogen phthalate was used as standard. The reproducibility of the analytical procedure was within 2–3 % for the current study.

2.4 Absorption measurement

In laboratory, all the samples were filtered at low pressure, first through a pre-combusted Whatman GF/F filter (0.7 µm) and then through a pre-rinsed 25 mm Millipore membrane cellulose filter (0.22 µm) into glass bottles. Absorption spectra of the samples were measured between 200 and 800 nm at 1 nm increments using a Shimadzu UV-2600PC UV-Vis dual beam spectrophotometer with a 1 cm quartz cuvette and Milli-Q water as reference. The absorption coefficient a_{CDOM} was calculated from the measured optical density (OD) of the sample using Eq. (1):

$$a_{CDOM}(\lambda) = 2.303 \left[OD_{S(\lambda)} - OD_{(null)}\right] / \gamma \quad (1)$$

where γ is the cuvette path length (0.01 m) and the factor 2.303 converts from base 10 to base natural logarithm transformation. Some fine particles possibly remained in the filtered solution (Babin et al., 2003; Bricaud et al., 1995), therefore it is necessary to correct for scattering by fine particles and in this case, $OD_{(null)}$ is the average optical density over 740–750 nm that the absorbance of CDOM can be assumed to be zero.

A CDOM absorption spectrum ($a_{CDOM}(\lambda)$) can be expressed as an exponential function (Babin et al., 2003; Bricaud et al., 1995):

$$a_{CDOM}(\lambda_i) = a_{CDOM}(\lambda_r) \exp\left[-S\left(\lambda_i - \lambda_r\right)\right] \quad (2)$$

where $a_{CDOM}(\lambda_i)$ is the CDOM absorption at a given wavelength λ_i, $a_{CDOM}(\lambda_r)$ is the absorption estimate at the reference wavelength λ_r (440 nm), and S is the spectral

BGD
12, 5725–5756, 2015

slope of the CDOM absorption. According to Helms et al. (2008), S is calculated by fitting a linear model to the date over a wavelength range of 275–295 nm (S1) or 350–400 nm (S2). To eliminate the inter-laboratory variability, the ratio $S_R = S1/S2$ is defined to indicate the contribution of different sources in terms of their molecular weights (Zhang et al., 2010).

2.5 Three-dimensional fluorescence measurement

EEMs of CDOM were measured using a Hitachi F-7000 fluorescence spectrometer (Hitachi High-Technologies, Tokyo, Japan) with a 700 voltage xenon lamp. The scanning ranges we used were 200–450 nm for excitation, and 250–500 nm for emission. Readings were collected in ratio mode at 5 nm intervals for excitation, and at 1 nm intervals for emission, using a scanning speed of 2400 nm min^{-1}. The band-passes were 5 nm for both excitation and emission. A Milli-Q water blank of the EEMs was subtracted to eliminate the water Raman scatter peaks (McKnight et al., 2001; Stemdon et al., 2003; Zhang et al., 2010, 2011).

The inner-filter effect is the major problem with EEMs measurement of CDOM because of the reabsorption of the exciting by the fluorescent itself (McKnight et al., 2001), which can reduce the intensity of fluorescent component by 5 % (Larsson et al., 2007). In order to eliminate the inner-filter effect, the EEMs were corrected for absorbance by multiplying each value in the EEMs with a correction factor based on the assumption that the average path length of absorption of the excitation and emission light is one-half length of the cuvette (McKnight et al., 2001; Zhang et al., 2010). The correction function is expressed as follows:

$$F_{corr} = F_{obs} \times 10^{(A_{ex}+A_{em}/2)} \quad (3)$$

where F_{corr} and F_{obs} are the corrected and uncorrected fluorescence intensities and A_{ex} and A_{em} are the absorbance values at the current excitation and emission wavelengths.

Finally, the fluorescence intensities in all sample EEMs were normalized to the area under the Milli-Q water Raman peak (λex = 350 nm, λem = 371–428 nm) collected daily

BGD
12, 5725–5756, 2015

(Lawaetz and Stedmon, 2009). The contour figures of the EEMs were plotted using the Matlab 10.0 software package (Math Works, Natick Massachusetts, America).

2.6 The PARAFAC modeling

Parallel factor analysis (PARAFAC), a three-way method, is applied to decompose EEMs of the complicate mixture CDOM into individual fluorescence groups and the model is written as (Andersen and Bro, 2003; Stedmon and Bro, 2008):

$$X_{ijk} = \sum_{f=1}^{F} a_{if} b_{jf} c_{kf} + \varepsilon_{ijk}$$
$$i = 1,\ldots,I;\ j = 1,\ldots,J;\ k = 1,\ldots,K \quad (4)$$

where F defines the number of components in the model, X_{ijk} is the intensity of fluorescence of the ith sample at the jth emission wavelength and kth excitation wavelength. In this study, a_{if} is linearly related to the concentration of fluorescence f in a sample I and b_{jf} is proportional to the fluorescence quantum efficiency of the fth analyte at an emission wavelength j; c_{kf} is the score for the fth component at the excitation wavelength j; ε_{ijk} is the residual matrix, and i, j, k represent the variability not accounted for by the relative model. A detailed description of the assumption for PARAFAC can be found in Stedmon and Bro (2008).

In our study, the PARAFAC procedure can be outlined as below: (1) the normalized excitation-emission matrixes were combined into a single Excel file consisting of 67 worksheets, (2) the excitation wavelengths from 200 to 220 nm and the emission wavelengths from 250 to 300 nm were deleted, (3) NaN was inserted in the regions $\mathrm{Ex}-20 \le \mathrm{Em} \le \mathrm{Ex}+20$ and $2\mathrm{Ex}-20 \le \mathrm{Em} \le 2\mathrm{Ex}+20$; unit: nm, (4) PARAFAC analysis was carried out in the "N-way DOMFluor toolbox for MATLAB".

A number of investigators have used EEMs and PARAFAC to characterize DOM in freshwater and marine aquatic environments (Cory et al., 2005; Stedmon et al., 2005; Yamashita, 2008; Zhang et al., 2010, 2011). According to Stedmon and Bro (2008),

BGD
12, 5725–5756, 2015

a similar PARAFAC analysis is carried out in the present study using the DOMFluor toolbox in MATLAB with the "N-way toolbox for MATLAB" (Andersso et al., 2000). Before PARAFAC modeling, the excitation wavelengths from 200 to 220 nm and the emission wavelengths from 250 to 300 nm were deleted because of their poor quality. Also, the Rayleigh scatter should be removed prior to PARAFAC modeling because the values do not describe DOM fluorophore in the area. In order to remove the Rayleigh scatter, the missing values (NaN-Not a number) should be inserted in the regions ($Ex - 20 \leq Em \leq Ex + 20$ and $2Ex - 20 \leq Em \leq 2Ex + 20$; unit: nm) which are significantly influenced by the first and second order scattering from the measured spectroscopic data (Hua et al., 2007; Stedmon and Bro, 2008).

Split-half analysis is the most important method included in the PARAFAC model, in which the EEMs are randomly divided into four groups of equal size, and then analyzed for two half splits (1–2 and 3–4 half) respectively. If the correct number of components is chosen, the excitation and emission loadings from the two groups of modeling should show the same shape and size (Bro et al., 1997, 1999). The fluorescence intensity of every component was represented by F_{max} (Raman unit: nm^{-1}) (Stedmon et al., 2005).

2.7 Statistical analysis

Statistical analyses were conducted using the SPSS 16.0 software package (Statistical Program for Social Sciences). Regression and correlation analyses (paired t test) were used to calculate the relationship between CDOM absorption coefficient, DOC concentration, salinity and F_{max}. The difference is considered to be statistically significant when p values are less or equal to 0.05.

BGD
12, 5725–5756, 2015

3 Results and discussion

3.1 Water quality conditions

The water quality parameters pH, salinity, turbidity for the 67 water samples collected from June 2013 to April 2014 in the western part of Jilin province are displayed in Table 1. When the whole set of samples were pooled together, the waters had high pH values (mean, 8.55) and high salt contents (mean, 0.48 PSU). When the lakes were frozen, the highest salinity 0.70 PSU was present in February 2014. The salinity for lakes with other three seasons was almost the same, which was about 0.40 PSU. Also the water bodies were highly turbid with the mean 62.18 ± 79.07 NTU. The highest turbidity was present in June 2013 with 166.20 ± 108.73 NTU, then reduced to 63.13 ± 31.21 NTU in August 2013 with rainfall increasing, and then reduced to the lowest 21.33 ± 15.87 NTU in February 2014. Compared with the turbidity in February 2014, the turbidity had almost no change in April 2014 with 22.24 ± 16.42 NTU.

3.2 EEMs characterization of CDOM

Based on the EEMs "peak picking" technique, four key fluorescence peaks can be observed in 67 water samples: two humic-like (Peaks A and C) and two protein-like (Peaks B and T) substances (Coble et al., 1996; Stedmon et al., 2003). The humic-like component is a complex mixture of aromatic and aliphatic compounds-fulvic acids and humic acids, which were originated from terrestrial materials or algal decomposition in the waters. While the two protein-like components consist of two dissolved amino acids, i.e., tryptophan and tyrosine that are originated from microbial activity (Baker et al., 2004; Hudson et al., 2007). Taking Xindianpao as an example with different seasons (Fig. 2), the peaks comprise two humic-like fluorescence components: A-humic-like (Ex/Em = 220–240/410–430 nm); C-humic-like (Ex/Em = 300–340/410–450 nm) and two protein-like fluorescence components: B-tyrosine-like (Ex/Em = 210–230, 270–280/310–330 nm); T-tryptophan-like (Ex/Em = 220–230, 280–

BGD
12, 5725–5756, 2015

300/350–370 nm). The measured peak intensity of these fluorescence centers is dependent on the concentration of the main fluorophores dissolved in water bodies.

To determine the appropriate number of PARAFAC components, the split-half validation procedure was executed to verify whether the model was valid by comparing the emission and excitation loadings from each half (Stedmon and Bro, 2008). In split-half analysis, the 67 EEMs were randomly divided into four halves and then analysized for two different splits (1–2 and 3–4 half split). When the number of components was chosen to be four, the excitation and emission loadings from the output results of 1–2 and 3–4 split-half analysis showed largely overlapped pattern, respectively (Fig. 3). It should be noted that for the 3–4 split-half analysis, the excitation and emission loadings of component 3 and component 4 were reversed. In fact, the output results of the split-half analysis were valid as long as the excitation and emission loadings of the fluorescence component were overlapped at the same wavelength and different colors of different components in the two groups only represent the order of appearance of the components according to their contributions (Stedmon and Bro, 2008).

In our study, four separate fluorescent components (Fig. 4a–d) and the excitation and emission loadings (Fig. 4e–h) of the four components identified by EEM-PARAFAC are summarized in Fig. 4 and Table 2. The first fluorescent component (C1) was a biological degradation humic-like component that displays two excitation maxima (at 230 and 300 nm) with a single emission wavelength (at 425 nm) comparable to humic-like peaks in marine and in phytoplankton degradation experiments for inland waters (Coble, 1996; Zhang et al., 2010). Compared with C1, the maximum excitation (at 255 and 350 nm) and an emission (at 460 nm) of component 2 shifted to the red spectral region (Fig. 4a and b), which was consistent with the humic-like peaks (A and C) defined by Coble (1996). Component 3 demonstrated two excitation maxima (at 225 and 290 nm) and one emission maximum (at 360 nm), which is considered to be similar to tryptophan. For component 4, it is likely related to tyrosine, which was characterized by maximum excitations at 220 and 275 nm and the emission wavelength was found at 320 nm. Components 3 and 4 represent autochthonous semi-labile CDOM associated with

BGD
12, 5725–5756, 2015

bacteria activity and phytoplankton degradation. Particularly, there was a shoulder at the excitation wavelength 310–330 nm in component 3 and 330–340 nm in component 4, which may be due to the residual Raman peaks in some water sample (Fig. 4c and d). However, these results from our study do not mean all the four components were shown in every water sample.

3.3 Temporal distribution of PARAFAC components

As shown in Fig. 5, the average fluorescence intensity of the four components differed with seasonal variation. When all the water samples in different seasons were pooled together, the average value of total fluorescence intensity was $2.05 \pm 0.93\,\mathrm{nm}^{-1}$, corresponding to the intensities of 0.71 ± 0.32 (C1), 0.33 ± 0.11 (C2), 0.50 ± 0.24 (C3), and $0.51 \pm 0.26\,\mathrm{nm}^{-1}$ (C4) for different components. The fluorescence intensity was dominated by peak C1, indicating that most part of CDOM for inland waters was originated from phytoplankton degradation. The lowest C2 intensity represented only a small portion of CDOM, which can be attributed to terrestrial import to water bodies. The two protein-like intensities (B and T), related to bioavailability and microbial activity of CDOM, had almost the same magnitude. The total fluorescence intensity significantly varied from $2.54 \pm 0.68\,\mathrm{nm}^{-1}$ in June to $1.93 \pm 0.70\,\mathrm{nm}^{-1}$ in August 2013, and then increased to $2.34 \pm 0.92\,\mathrm{nm}^{-1}$ in February and reduced to the lowest $1.57 \pm 0.55\,\mathrm{nm}^{-1}$ in April 2014. In June 2013, the intensities of four fluorescence components (0.75 ± 0.17 (C1), 0.32 ± 0.06 (C2), 0.69 ± 0.24 (C3), $0.77 \pm 0.20\,\mathrm{nm}^{-1}$ (C4)) exhibited the similar trends to the whole set of samples, but higher than the average except the C2 $0.32 \pm 0.06\,\mathrm{nm}^{-1}$. This can be explained by enhanced activities from plant degradation and others. Compared to the fluorescence intensity in June, the three fluorescence intensities 0.65 ± 0.14 (C1), 0.33 ± 0.16 (C3), $0.52 \pm 0.36\,\mathrm{nm}^{-1}$ (C4) from samples collected in August 2013 reduced, but an increased intensity of C2 ($0.42 \pm 0.05\,\mathrm{nm}^{-1}$) was recorded. Especially, the two protein-like peaks showed obvious difference. From June to August 2013, the precipitation substantially increased up to 180 mm in July (Fig. 6b) so that the flood occurred when the rainfall continued to

BGD
12, 5725–5756, 2015

increase in August. The fluorescence intensity of rainwater was mostly characterized by protein-like components and lower humic-like concentration (Fig. 7b) (Cheng et al., 2010). Gradually, DOM contained in terrestrial CDOM was flushed by the rainfall to the lakes so that the C2 ($0.42 \pm 0.05\,nm^{-1}$) fluorescence intensity gradually became higher but all the intensities of the other three peaks decreased because of dilution with a lot of rain and so weakened active microbial decomposition of plants.

The highest C1 ($1.02 \pm 0.38\,nm^{-1}$) presented in February 2014 and the C2 ($0.39 \pm 0.12\,nm^{-1}$) intensity maintained almost the same as that in August 2013. However, the two protein-like peaks indicated that the C3 ($0.57 \pm 0.25\,nm^{-1}$) intensity was higher than the C4 ($0.35 \pm 0.17\,nm^{-1}$) intensity, which was opposite to the results from other months. In deep winter, the surface waters, after frozen, formed with a thick layer of ice covering the lake waters and strong biological activities in waters would be prohibited, therefore the C1 and C3 in the waters beneath the ice layers would cumulate simultaneously. Obviously, the fluorescence intensity of component 1 reached to the highest value of $1.02 \pm 0.38\,nm^{-1}$. As shown in Fig. 6a, another striking feature for winter samples was that the ice CDOM fluorescence was dominated by the protein-like C4 peaks, which is consistent with the finding of Barker et al. (2009, 2013) and Stedmon et al. (2007). It is not surprising that the intensity of peak B for water beneath ice layer was reduced and the concentrated C3 showed higher fluorescence intensity of $0.57 \pm 0.25\,nm^{-1}$. In April 2014, the intensities of four fluorescence components (0.47 ± 0.17 (C1), 0.25 ± 0.08 (C2), 0.40 ± 0.16 (C3), $0.45 \pm 0.13\,nm^{-1}$ (C4)) characterized by the similar trends with the whole but lower than the average. Our interpretation is that the ice in the lakes melt into water with the weather warming and the biological degradation and human activity was weak, CDOM was diluted and the fluorescence intensity reached to the lowest values.

Compared with previous works by Borisover et al. (2009) and Zhang et al. (2011), our study identifies the humic-like component 1 and 2, and the two protein-like components such as tyrosine-like and tryptophan-like peaks in CDOM for lakes in semi-arid region of Northeast China with obviously seasonal characteristics. Especially in summer when

BGD
12, 5725–5756, 2015

quantities of rainfall taking place and in winter when water is frozen, the fluorescence intensity is dominated by tyrosine-like peak B in rain and ice-melt water.

3.4 CDOM vs. EEM-PARAFAC extracted components

The water quality parameters DOC concentration, salinity and absorption coefficient are shown in Table 3. For the 67 water samples, the DOC concentration ranged from 10.03 to 88.15 $mg\,L^{-1}$ during the study period, with an average value of $37.60 \pm 18.05\,mg\,L^{-1}$, demonstrating a seasonal dynamics that can be attributed to hydrological, climatic and landscape variation (Song et al., 2013). Generally, the absorption coefficient a(350) was used as an proxy for characterizing CDOM concentration, which was $5.73 \pm 1.68\,m^{-1}$ in June 2013, $5.82 \pm 0.81\,m^{-1}$ in August 2013, $6.36 \pm 2.17\,m^{-1}$ in February 2014, $4.17 \pm 1.49\,m^{-1}$ in April 2014, respectively, with an average of $5.40 \pm 1.84\,m^{-1}$ when the data were pooled together. The highest CDOM absorption coefficients a(350) $6.36 \pm 2.17\,m^{-1}$, a(280) $34.62 \pm 11.54\,m^{-1}$, a(254) $52.88 \pm 18.13\,m^{-1}$ were present in February 2014, corresponding to the highest DOC concentration of $55.04 \pm 20.00\,mg\,L^{-1}$. This can be attributed to the accumulated dissolved organic carbon when lakes freeze in winter, which expels DOC from ice, resulting in a high DOC concentration in the underlying water (unpublished material). Also, the spectral ratio (S_R) of the two wavelength ranges (275–295 nm over 350–400 nm) was used to represent the ratio of molecular weight of humic acid and fulvic acid. The mean of spectral ratio (S_R) for all water samples was up to 1.21 ± 0.20, with the lowest 0.96 ± 0.22 in August 2013 which indicated the higher activities of biology and others resulting in decomposition of higher molecule carbon into lower molecule.

When the whole data set ($N = 67$) was pooled together, there were significantly positive linear relationships between a(254), a(280), a(350) and F_{max} for two humic-like components (C1 and C2), respectively, but mostly such correlations were not observed for the protein-like peaks (Fig. 7, Table 3). These results were in accordance with some published literatures (Zhang et al., 2010, 2011). Components 1 and 2 were strongly linearly correlated with each other ($R^2 = 0.633$), indicating that the concentrations of

BGD
12, 5725–5756, 2015

the two humic-like components were controlled by common sources. There was a weak relationship (R^2 = 0.051) between the two protein-like peaks (B and T) because of the effects of rainfall in summer, ice in winter and other human waste, which represent the complex origins of CDOM. However, almost no correlation between humic-like peaks and protein-like peaks shows that the two components were derived from different sources. The linkage of a fluorescence signal to DOC was very complicated because of the effects of both steady and labile fluorescence and non-fluorescence CDOM with seasonal impacts such as increased rainfall and algal blooms which affect the DOC concentration (Henderson et al., 2009). A weak relationship (R^2 = 0.42) (Fig. 7d) was found between DOC and component 3 from the decay of plants through microbial activity or the pollution from human and animal wastes, indicating that the component 3 of the CDOM fluorescence (protein-like peak T) can be used to detect water pollution (Baker et al., 2004).

The most important finding for waters with seasonal variation in the western part of Jilin province is a significant relationship (R^2 = 0.931) observed between salinity and DOC (Fig. 7e), which implies that the prolonged sunshine duration can result in an evapo-condensed DOC concentration. Different from the findings from Yamashita (2008), this study did not find obvious correlation between salinity and EEM-PARAFAC extracted components except C3 (R^2 = 0.469) (Table 4 and Fig. 7d). It was because that with the sunshine duration hours increasing, the photo-degradation and microbial activities become stronger, leading to the more transformation of labile fluorescence CDOM into non-fluorescence CDOM component (Song et al., 2013).

4 Conclusions

In this study, the application of excitation-emission matrices fluorescence and parallel factor analysis (EEM-PARAFAC) to characterize the seasonal variation of four fluorescence components in CDOM was presented for 67 water samples collected from July 2013 to April 2014 in the semi-arid region of Northeast China. Two humic-

BGD
12, 5725–5756, 2015

like peaks (C1 Ex/Em = 230 (300)/425 nm and C2 Ex/Em = 255 (350)/460 nm) and two protein-like (B Ex/Em = 220 (275)/320 nm and T Ex/Em = 225 (290)/360 nm) peaks were identified using PARAFAC model. The average fluorescence intensity of the four components differed with seasonal variation from July 2013 to April 2014. In general, the fluorescence intensity was dominated by peak C1 indicating that most part of CDOM for inland waters was originated from phytoplankton degradation. The lowest C2 represents only a small portion of CDOM from terrestrial import to water bodies through rainwash and soil leaching. The two protein-like intensities (B and T) have almost the same magnitude. Especially, in August 2013 and in February 2014, the two protein-like peaks showed obviously different and the highest C1 1.02 nm^{-1} presented in February 2014. Component 1 and 2 exhibited strong linear correlation (R^2 = 0.633) indicating that the concentrations of the two humic-like components were controlled by common sources. There were significantly positive linear relationships between F_{max} and CDOM absorption coefficient a(254) (R^2 = 0.72, 0.46, $p < 0.01$), a(280) (R^2 = 0.77, 0.47, $p < 0.01$), a(350) (R^2 = 0.76, 0.78, $p < 0.01$) for two humic-like components (C1 and C2), respectively. A weak relationship (R^2 = 0.42) was found between DOC and component 3 from the decay of plants through microbial activity or the pollution from human and animal wastes which indicated that the components 3 (protein-like peak T) can detect lake pollution derived from fluorescence CDOM. Most importantly, a close relationship (R^2 = 0.931) was found between salinity and DOC. However, almost no obvious correlation was found between salinity and EEM-PARAFAC extracted components except C3 (R^2 = 0.469), though the correlation was not as strong as with DOC concentration.

Acknowledgements. This research was jointly supported by the "One Hundred Talents" program from Chinese Academy of Sciences and the National Natural Science Foundation of China (No. 41 471 290 and 41 171 293).The authors thank Zhi Ding, Ying Guan, Lei Liu and Ming Wang for their persistent assistance with both field sampling and laboratory analysis.

BGD
12, 5725–5756, 2015

References

Aiken, G. R., McKnight, D. M., Thorn, K. A., and Thurman, E. M.: Isolation of hydrophobic organic-acids from water using nonionic macro porous resins, Org. Geochem., 18, 567–573, 1992.

Andersson, C. A. and Bro, R.: The N-way Toolbox for MATLAB, Chemometr. Intell. Lab., 52, 1–4, 2000.

Andersen, C. M. and Bro, R.: Practical aspects of PARAFAC modeling of fluorescence excitation-emission data, J. Chemometr., 17, 200–215, 2003.

Babin, M., Stramski, D., Ferrari, G. M., Claustre, H., Bricaud, A., Obolensky, G., and Hoepffner, N.: Variations in the light absorption coefficients of phytoplankton, nonalgal particles, and dissolved organic matter in coastal waters around Europe, J. Geophys. Res., 108, 3211–3230, 2003.

Baker, A., Ward, D., Lieten, Shakti, H., Periera, R., Simpson, Ellie, C., and Slater, M.: Measurement of protein-like fluorescence in river and waste water using a handheld spectrophotometer, Water Res., 38, 2934–2938, 2004.

Barker, J. D., Sharp, M. J., Fitzsimons, S. J., and Turner, R. J.: Abundance and dynamics of dissolved organic carbon in glacier systems, Arct. Antarct. Alp. Res., 38, 163–172, 2006.

Barker, J. D., Sharp, M. J., and Turner, R. J.: Using synchronous fluorescence spectroscopy and principal components analysis to monitor dissolved organic matter dynamics in a glacier system, Hydrol. Process., 23, 1487–1500, 2009.

Barker, J. D., Klassen, J. L., Sharp, M. J., Fitzsimons, S. J., and Turner, R. J.: Detecting biogeochemical activity in basal ice using fluorescence spectroscopy, Ann. Glaciol., 51, 47–55, 2010.

Barker, J. D., Dubnick, A., Lyons, W. B., and Chin, Y. P.: Changes in Dissolved Organic Matter (DOM) fluorescence in proglacial antarctic streams, Arct. Antarct. Alp. Res., 45, 305–317, 2013.

Borisover, M., Laor, Y., Parparov, A., Bukhanovsky, N., and Lado, M.: Spatial and seasonal patterns of fluorescent organic matter in Lake Kinneret (Sea of Galilee) and its catchment basin, Water Res., 43, 3104–3116, 2009.

Bricaud, A., Babin, M., Morel, A., and Claustre, H.: Variability in the chlorophyll-specific absorption coefficients of natural phytoplankton: analysis and parameterization, J. Geophys. Res., 100, 13321–13332, 1995.

BGD
12, 5725–5756, 2015

Bro, R.: PARAFAC tutorial and applications, Chemometr. Intell. Lab., 38, 149–171, 1997.
Bro, R.: Exploratory study of sugar production using fluorescence spectroscopy and multi-way analysis, Chemometr. Intell. Lab., 46, 133–147, 1999.
Cheng, Y. Y., Guo, W. D., Long, A. M., and Chen, S. Y.: Study on optical characteristic of chromophoric dissolved organic matter in rainwater by fluorescence excitation-emission matrix and absorbance spectroscope (in Chinese), Spectrosc. Spect. Anal., 30, 2413–2416, 2010.
Coble, P. G.: Characterization of marine and terrestrial DOM in seawater using excitation-emission matrix spectroscopy, Mar. Chem., 51, 325–346, 1996.
Coble, P. G.: Marine optical biogeochemistry: the chemistry of ocean color, Chem. Rev., 107, 402–418, 2007.
Coble, P. G., Del Castillo, C. E., and Avril, B.: Distribution and optical of CDOM in the Arabian Sea during the 1995 Southwest Monsoon, Deep-Sea Res. Pt. II, 45, 2195–2223, 1998.
Cory, R. M. and McKnight, D. M.: Fluorescence spectroscopy reveals ubiquitous presence of oxidized and reduced quinines in dissolved organic matter, Environ. Sci. Technol., 39, 8142–8149, 2005.
DelCastillo, C. E., Coble, P. G., Morell, J. M., Lopez, J. M., and Corredor, J. E.: Analysis of the optical properties of the Orinoco River plume by absorption and fluorescence spectroscopy, Mar. Chem., 66, 35–51, 1999.
Duarte, C. M., Montes, C., Cole, J. J., Striegl, R. G., Melackand, J., and Downing, J. A.: CO_2 emissions from saline lakes: a global estimate of a surprisingly large flux, J. Geophys. Res., 113, G04041, doi:10.1029/2007JG000637, 2008.
Fellman, J. B., Hood, E., and Spencer, R. G. M.: Fluorescence spectroscopy opens new windows into dissolved organic matter dynamics in freshwater ecosystems: a review, Limnol. Oceanogr., 55, 2452–2462, 2010.
Guo, W. D., Xu, J., Wang, J. P., Wen, Y. G., Zhou, J. F., and Yan, Y. C.: Characterization of dissolved organic matter in urban sewage using excitation emission matrix fluorescence spectroscopy and parallel factor analysis, J. Environ. Sci., 22, 1728–1734, 2010.
Helms, J. R., Stubbins, A., Ritchie, J. D., Minor, E. C., Kieber, D. J., and Mopper, K.: Absorption spectral slopes and slope ratios as indicators of molecular weight, source, and photo bleaching of chromophoric dissolved organic matter, Limnol. Oceanogr., 53, 955–969, 2008.

BGD
12, 5725–5756, 2015

Henderson, R. K., Baker, A., Murphy, K. R., Hambly, A., Stuetz, R. M., and Khan, S. J.: Fluoresence as a potential monitoring tool for recycled water system: a review, Water Res., 43, 863–881, 2009.
Hua, B., Dolan, F., Mcghee, C., Clevenger, Thomas, E., and Deng, B. L.: Water-source characterization and classification with fluorescence EEM spectroscopy: PARAFAC analysis, Int. J. Environ. An. Ch., 87, 135–147, 2007.
Hudson, N., Baker, A., and Reynolds, D.: Fluorescence analysis of dissolved organic matter in natural, waste and polluted waters – a review, River Res. Appl., 23, 631–649, 2007.
Jaffé, R., Boyer, J. N., Lu, X., Maie, N., Yang, C., Scully, N. M., and Mock, S.: Source characterization of dissolved organic matter in subtropical mangrove-dominated estuary by fluorescence analysis, Mar. Chem., 84, 195–210, 2004.
Larsson, T., Wedborg, M., and Turner, D.: Correction of inner-filter effect in fluorescence excitation-emission matrix spectrometry using Raman scatter, Anal. Chim. Acta, 583, 357–363, 2007.
Lawaetz, A. J. and Stedmon, C. A.: Fluorescence intensity calibration using the Raman Scatter Peak of Water, Appl. Spectrosc., 63, 936–940, 2009.
Mayer, L. M., Schick, L. L., and Loder, T. C.: Dissolved protein fluorescence in two Maine estuaries, Mar. Chem., 64, 171–179, 1999.
Mcknight, D. M., Boyer, E. W., Westerhoff, P. K., Doran, P. T., Kulbe, T., and Andersen, D. T.: Spectrofluorometric characterization of dissolved organic matter for indication of precursor organic material and aromaticity, Limnol. Oceanogr., 46, 38–48, 2001.
Song, K. S., Zang, S. Y., Zhao, Y., Li, L., Du, J., Zhang, N. N., Wang, X. D., Shao, T. T., Guan, Y., and Liu, L.: Spatiotemporal characterization of dissolved carbon for inland waters in semi-humid/semi-arid region, China, Hydrol. Earth Syst. Sci., 17, 4269–4281, doi:10.5194/hess-17-4269-2013, 2013.
Spencer, R. G. M., Hernes, P. J., Ruf, R., Baker, A., Dyda, R. Y., Stubbins, A., and Six, J.: Temporal controls on dissolved organic matter and lignin biogeochemistry in apristine tropical river, J. Geophys. Res., 115, G03013, doi:10.1029/2009JG001180, 2010.
Stedmon, C. A. and Bro, R.: Characterizing dissolved organic matter fluorescence with parallel factor analysis: a tutorial, Limnol. Oceanogr.-Meth., 6, 572–579, 2008.
Stedmon, C. A. and Markager, S.: Tracing the production and degradation of autochthonous fractions of dissolved organicmatter by fluorescence analysis, Limnol. Oceanogr., 50, 1415–1426, 2005.

BGD
12, 5725–5756, 2015

Stedmon, C. A., Markager, S., and Bro, R.: Tracing dissolved organic matter in aquatic environments using a new approach to fluorescence spectroscopy, Mar. Chem., 82, 239–254, 2003.

Stedmon, C. A., Thomas, D. N., Granskog, M., Kaartokallio, H., Papadimitriou, S., and Kuosa, H.: Characteristics of dissolved organic matter in Baltic coastal sea ice: allochthonous or autochthonous origins?, Environ. Sci. Technol., 41, 7273–7279, 2007.

Tranvik, L. J., Downing, J. A., Cotner, J. B., Loiselle, S. A., Striegl, R. G., Ballatore, T. J., Dillon, P., Finlay, K., Fortino, K., Knoll, L. B., Kortelainen, P. L., Kutser, T., Larsen, S., Laurion, I., Leech, D. M., McCallister, S. L., McKnight, D. M., Melack, J. M., Overholt, E., Porter, J. A., Prairie, Y., Renwick, W. H., Roland, F., Sherman, B. S., Schindler, D. W., Sobek, S., Tremblay, A., Vanni, M. J., Verschoor, A. M., Wachenfeldt, E. V., and Weyhenmeyer, G. A.: Lakes and reservoirs as regulators of carbon cycling and climate, Limnol. Oceanogr., 54, 2298–2314, 2009.

Yamashita, Y.: Assessing the dynamics of dissolved organic matter (DOM) in coastal environments by excitation emission matrix fluorescence and parallel factor analysis (EEM-PARAFAC), Limnol. Oceanogr., 53, 1900–1908, 2008.

Yamashita, Y., Cory, R. M., Nishioka, J., Kuma, K., Tanoue, E., and Jaffé, R.: Fluorescence characteristics of dissolved organic matter in the deep waters of the Okhotsk Sea and the northwestern North Pacific Ocean, Deep-Sea Res. Pt. II, 57, 1478–1485, 2010.

Zhang, Y. L., Zhang, E. L., Yin, Y., VanDijk, M. A., Feng, L. Q., Shi, Z. Q., Liu, M. L., and Qin, B. Q.: Characteristics and sources of chromophoric dissolved organic matter in lakes of the Yungui Plateau, China, differing in trophic state and altitude, Limnol. Oceanogr., 55, 2645–2659, 2010.

Zhang, Y. L., Yin, Y., Feng, L. Q., Zhu, G. W., Shi, Z. Q., Liu, X. H., and Zhang, Y. Z.: Characterizing chromophoric dissolved organic matter in Lake Tianmuhu and its catchment basin using excitation-emission matrix fluorescence and parallel factor analysis, Water Res., 45, 5110–5122, 2011.

Zhang, Y. L., Liu, X. H., Osburn, C. L., Wang, M. Z., Qin, B. Q., and Zhou, Y. Q.: Photo bleaching response of different source of chromophoric dissolved organic matter exposed to natural solar radiation using absorption and excitation-emission matrix spectra, PLoS ONE, 8, e77515, doi:10.1371/journal.pone.0077515, 2013.

BGD
12, 5725–5756, 2015

Table 1. Mean value of water quality parameters from June 2013 to April 2014. Turb denotes water turbidity; *N* denotes sampling numbers.

Item	pH	Salinity (PSU)	Turb (NTU)	*N*
Jun 2013	8.54	0.40	166.20 ± 108.73	15
Aug 2013	8.63	0.37	63.13 ± 31.21	13
Feb 2014	8.35	0.70	21.33 ± 15.87	17
Apr 2014	8.67	0.43	22.24 ± 16.42	22
All	8.55	0.48	62.18 ± 79.07	67

BGD
12, 5725–5756, 2015

Table 2. Positions of the fluorescence maximum peaks of the four components identified by PARAFAC model in the present study compared with those previously identified. Secondary excitation band is given in brackets.

Component No	Exmax (nm)	Emmax (nm)	Description and source	Label 1	Label 2
C1	230 (300)	425	Marine humic-like (phytoplankton degradation)	M	6
C2	255 (350)	460	Terrestrial humic-like	A and C	1 and 4
C3	225 (290)	360	Autochthonous tryptophan-like	T	
C4	220 (275)	320	Autochthonous tyrosine-like	B	8

Fluoresence peaks were named as Label 1 by Coble et al. (1996, 1998) and Zhang et al. (2010, 2011), while as Lable 2 by Stedmon and Markager (2005).

BGD
12, 5725–5756, 2015

Table 3. Mean values of DOC concentration and CDOM absorption coefficients groups with different seasons. S_R: the spectral slope ratio of $S_{275–295\,nm}$: $S_{350–400\,nm}$.

Item	a(254) m^{-1}	a(280) m^{-1}	a(350) m^{-1}	S_R	DOC $mg^{-1}\,L^{-1}$	N
Jun 2013	38.39 ± 9.23	25.98 ± 6.38	5.73 ± 1.68	1.29 ± 0.16	31.84 ± 14.67	15
Aug 2013	29.71 ± 4.73	19.36 ± 2.91	5.82 ± 0.81	0.96 ± 0.22	32.83 ± 14.78	13
Feb 2014	52.88 ± 18.13	34.62 ± 11.54	6.36 ± 2.17	1.18 ± 0.11	55.04 ± 20.00	17
Apr 2014	34.43 ± 11.38	22.45 ± 7.36	4.17 ± 1.49	1.32 ± 0.13	30.86 ± 10.91	22
All	39.08 ± 14.73	25.73 ± 9.58	5.40 ± 1.84	1.21 ± 0.20	37.60 ± 18.05	67

BGD
12, 5725–5756, 2015

Table 4. Correlation coefficients (R) and significance levels (p) of the linear relationships between CDOM absorption, DOC, salinity and fluorescence components.

	a(254)	a(280)	a(350)	DOC	Salinity	C1	C2	C3	C4
DOC	0.711**	0.646**	0.294*	1.000**					
Salinity	0.650**	0.579**	0.159	0.965**	1.000**				
C1	0.850**	0.875**	0.873**	0.496**	0.383**	1.000**			
C2	0.677**	0.686**	0.885**	0.414**	0.270*	0.796**	1.000**		
C3	0.452**	0.417**	0.134	0.648**	0.685**	0.267*	0.103	1.000**	
C4	−0.040	−0.016	0.078	−0.101	0.135	0.084	0.069	0.225	1.000**

* $p < 0.05$ level; ** $p < 0.01$ level.

BGD
12, 5725–5756, 2015

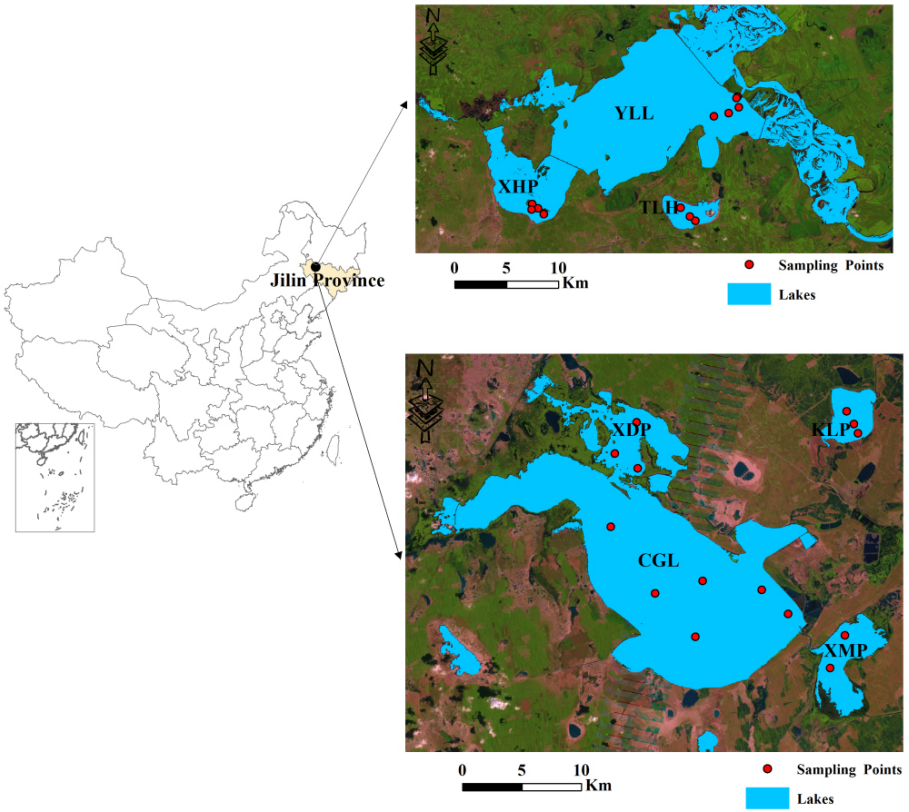

Figure 1. Locations of the water sampling sites for 7 lakes in the western part of Jilin province, Northeast China.

BGD
12, 5725–5756, 2015

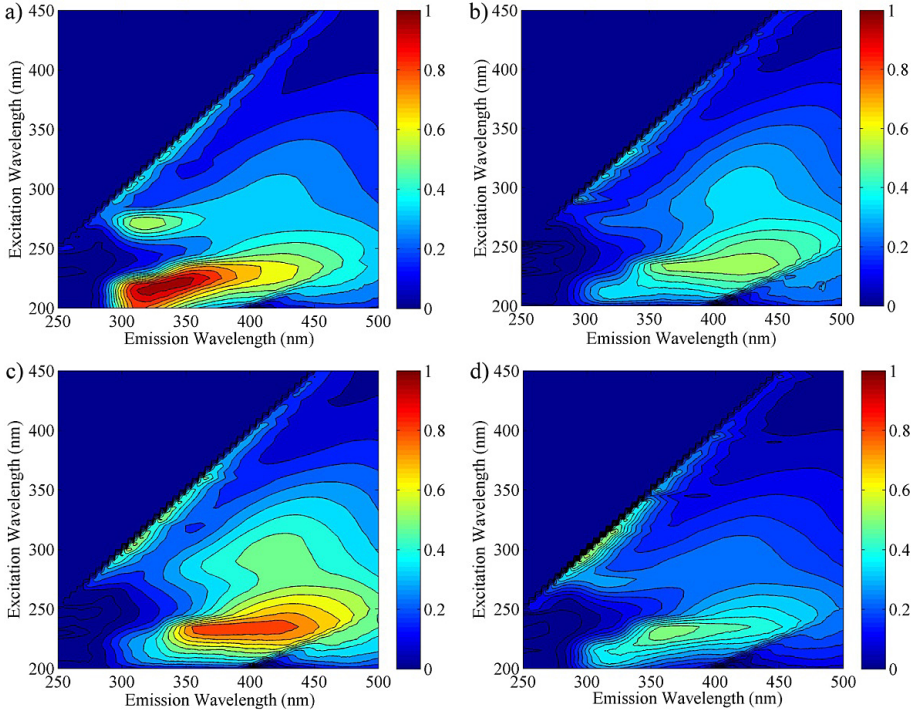

Figure 2. Examples of EEMs for one water sample from Xindianpao Lake in the western part of Jilin province from different seasons **(a)** June 2013; **(b)** August 2013; **(c)** February 2014; **(d)** April 2014 (Raman: nm^{-1}).

BGD
12, 5725–5756, 2015

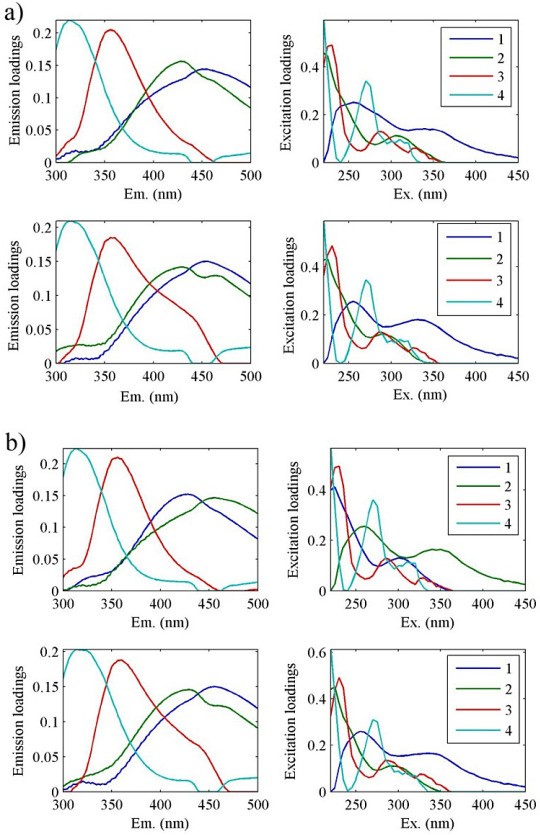

Figure 3. Results from split-half analysis (1–2 left; 3–4 right) in PARAFAC models. The plots represent spectral shapes of the excitation and emission loadings from the two halves (1–2; 3–4 split-half analysis) modeling.

BGD
12, 5725–5756, 2015

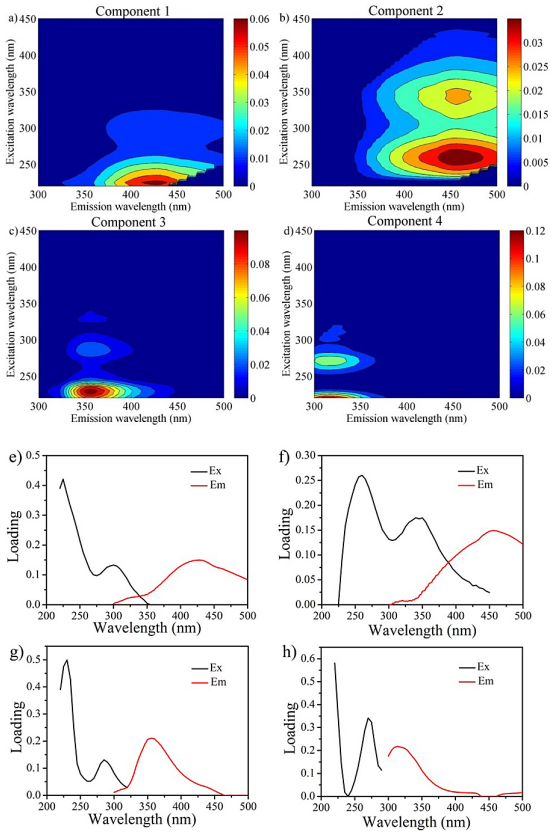

Figure 4. The PARAFAC model output showing fluorescence signatures of the four fluorescence components (**a**–**d**), the contour plots represent spectral shapes of excitation and emission. The line plots represent split-half validation results (**e**–**h**): excitation (left) and emission (right) spectra.

BGD
12, 5725–5756, 2015

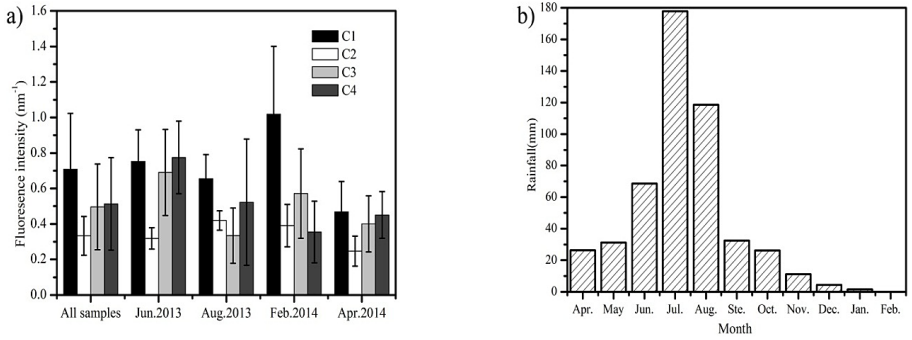

Figure 5. (a) Seasonal variation of F_{max} values of the four components (C1, C2, C3 and C4) for lakes in the western part of Jilin province; **(b)** monthly variation of rainfall for the lakes in the western part of Jilin province from April 2013 to February 2014. The error bar represents SD.

BGD
12, 5725–5756, 2015

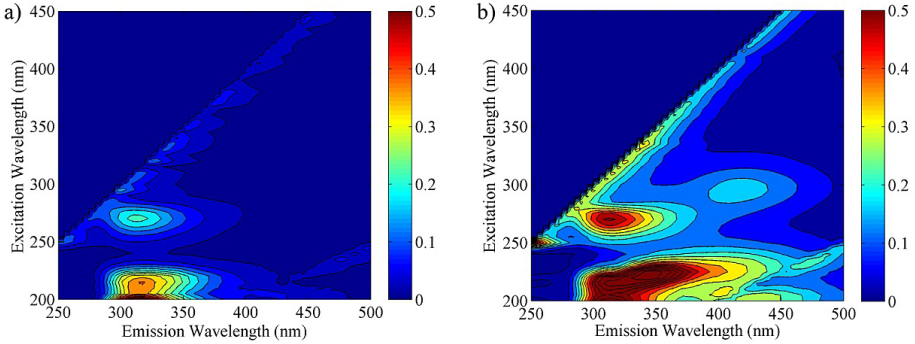

Figure 6. Representative examples of EEMs for **(a)** lake ice-melted water sample, and **(b)** rainwater CDOM in the western part of Jilin province (Raman: nm^{-1}).

BGD
12, 5725–5756, 2015

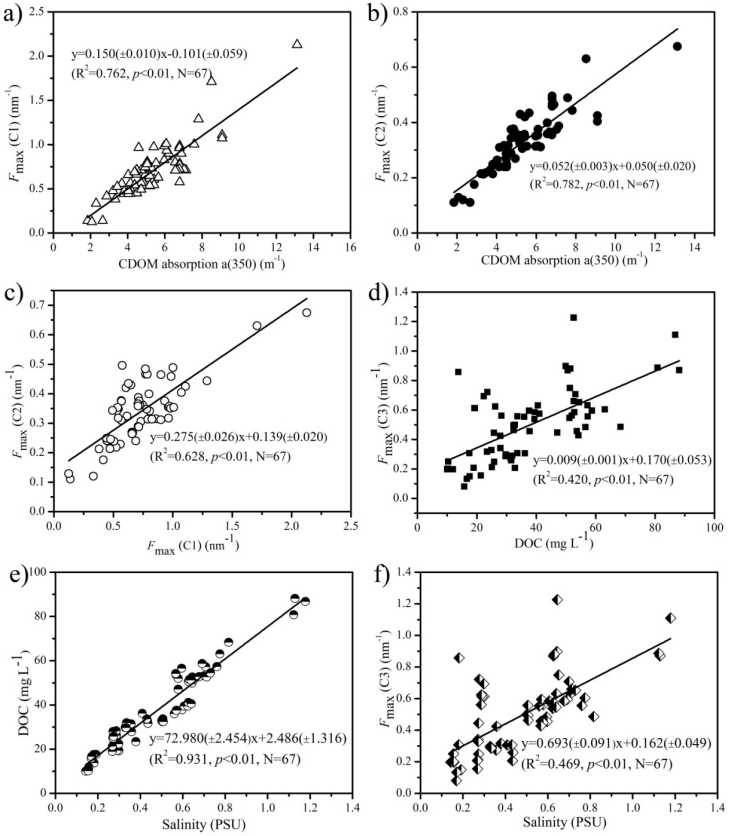

Figure 7. Relationships between CDOM absorption coefficient a(350) with **(a)** F_{max} (C1), **(b)** with F_{max} (C2), **(c)** peak F_{max} (C1) vs. F_{max} (C2), **(d)** peak F_{max} (C3) vs. DOC, **(e)** salinity vs. DOC, **(f)** salinity vs. F_{max} (C3).

BGD
12, 5725–5756, 2015